FULL-SCALE TESTING OF AN OGEE TIP ROTOR

Wayne R. Mantay
Structures Laboratory, U.S. Army R&T Laboratories (AVRADCOM)

Richard L. Campbell and Phillip A. Shidler
NASA Langley Research Center

SUMMARY

Full-scale tests were utilized to investigate the effect of the Ogee tip on helicopter rotor acoustics, performance, and loads. Two facilities were used for this study: the Langley whirl tower and a UH-1H helicopter. The test matrix for hover on the whirl tower involved thrust values from 0 to 44 480 N (10 000 lb) at several tip Mach numbers for both standard and Ogee rotors. The full-scale testing on the UH-1H encompassed the major portion of the flight envelope for that aircraft. Both near-field acoustic measurements and far-field flyover data were obtained for both the Ogee and standard rotors. Data analysis of the whirl-tower test shows that the Ogee tip does significantly diffuse the tip vortex while providing some improvement in hover performance at low and moderate thrust coefficients. Flight testing of both rotors indicates that the strong impulsive noise signature of the standard rotor can be reduced with the Ogee rotor. Analysis of the spectra indicates a reduction in energy in the 250 Hz and 1000 Hz range for the Ogee rotor. Forward-flight performance was significantly improved with the Ogee configuration for a large number of flight conditions. Further, rotor control loads were reduced through use of this advanced-tip rotor.

INTRODUCTION

The present day helicopter's usefulness and effectiveness is reduced by the high noise and vibration levels it generates. The increasing use of helicopters for military and commercial purposes necessitates a reduction in vibration as well as internal and external noise levels for reduced detection and community and passenger acceptance.

The interaction of a rotor blade tip vortex with the following blades is a major cause of increased helicopter acoustic signature, vibration, and loads (ref. 1). Numerous methods of reducing this vortex-blade interaction have been investigated in the past. One method, tip-shape modification, has shown some promise in reducing the severity of this phenomenon. One of the more promising tip configurations is the Ogee planform (fig. 1). Previous small-scale smoke studies indicated that this shape would diffuse the rotor blade tip vortex, and following blades might thus encounter a weaker vortex field with accompanying benefits. The Ogee tip shape (ref. 1) was evaluated by a series of analytical and experimental programs (refs. 2-5). Based on the encouraging results of the vortex flow data, pressure data, and performance information from these preliminary studies, full-scale testing of this tip shape was initiated.

Tests were conducted to investigate the effect of the Ogee tip on full-scale rotor acoustics, performance, and loads. The Langley whirl tower was utilized for hover flight measurements, and an extensively instrumented UH-1H provided forward-flight data.

SYMBOLS

Values are given in both S.I. and U.S. Customary Units. The measurements and calculations were made in U.S. Customary Units.

a	local speed of sound, m/sec
C_L	rotor lift coefficient, $\frac{GW}{\rho\pi R^2(\Omega R)^2}$
C_P	engine power coefficient, $\frac{P}{\rho\pi R^2(\Omega R)^3}$
C_Q	rotor torque coefficient, $\frac{Q}{\rho\pi R^3(\Omega R)^2}$
C_T	rotor thrust coefficient, $\frac{T}{\rho\pi R^2(\Omega R)^2}$
GW	helicopter gross weight, N (lb)
M_{TIP}	rotor tip Mach number, $\frac{\Omega R}{a}$
n	rotor load factor, g
OASPL	overall sound pressure level, dB
P	engine power, N-m/sec
Q	rotor torque, N-m
R	rotor radius, m (ft)
R/D	rate of descent, m/sec (ft/min)
T	rotor thrust, N
V_t	true airspeed, knots
z	height of aircraft above array center microphone, m

ρ local air mass density, kg/m^3

Ω rotor rotational speed, rad/sec

Superscript

$\overline{\quad}$ mean value

Subscript

o standard sea level condition

METHOD OF APPROACH

A systematic and controlled investigation of the effect of an advanced tip shape on rotor acoustics, loads, and performance was conducted on an Ogee tip rotor and a standard UH-1H square-tip rotor. Test facilities used for this study included the NASA-Langley whirl tower, an instrumented UH-1H helicopter, and the acoustic range at NASA Wallops Flight Center. Both near- and far-field acoustic data were obtained, as well as rotor performance, loads data, and wake flow visualization.

Description of Test Facilities and Hardware

Whirl tower.- The Langley helicopter rotor test facility (hereinafter referred to as the Langley whirl tower) has the capability of testing rotors through a complete hover envelope of thrust and rotational speed. The characteristics of this facility are shown in figure 2 and table I. The tower was used to verify the structural integrity of the Ogee design as well as provide performance, acoustics, and flow visualization.

Test helicopter.- The test vehicle for this investigation was a UH-1H helicopter. As shown in figure 3, the vehicle was equipped with electronic data systems, including an in-flight acoustic measurement system. Nominal test weights for the UH-1H were 33 805 N (7600 lb) and 38 253 N (8600 lb). The aircraft was flown with a crew of four, resulting in a nominal longitudinal center of gravity location 17.8 cm (7 in.) aft of the main rotor hub.

Rotor systems.- The geometric characteristics of both standard and Ogee rotors used in the tests are given in table II. Two sets of each rotor were used, one set of each for the tower investigation and one set of each for flight testing on the same test helicopter. Figure 4 shows the planform of both the standard rotor and Ogee tip rotor blades.

NASA Wallops Flight Center acoustic range.- An acoustic array was used to measure far-field noise from the helicopter. This array was located at the approach end of runway 10. Radar was used to track the vehicle over the approach to the array.

Description of Instrumentation

Whirl-tower data acquisition.- The parameters directly measured by the whirl-tower data system are listed in table III. Performance data as well as blade structural data were monitored in real time and recorded on FM tape. Acoustic data were obtained through an electronic system identical to that used in the Wallops Flight Center acoustic instrumentation, to be discussed later in this paper, with one microphone placed 76.2 m (250 ft) from the center of the tower on a ground board.

Helicopter instrumentation.- The UH-1H helicopter utilized three unique data systems. One onboard data package recorded and telemetered select helicopter parameters which included vehicle aerodynamic state, attitudes, powertrain data, rotor structural information, and vibratory loads. Table IV lists these parameters and the measurement techniques used. A second onboard data system digitally sampled tip pressures, strain-gage information, and rotor azimuth on the Ogee rotor. The electronics of this system were imbedded in the Ogee tip and enabled sampling rates as high as 2000 Hz to be obtained.

The in-flight acoustic measurement system (IFAMS) measured and recorded the near-field pressure signature of the test helicopter in various flight conditions. The system consists of two externally mounted microphones. The location of these is shown on figure 3. The condenser microphones, fitted with a streamlined nose section, could be adjusted ±10 degrees from centerline into the resultant local airflow. The microphone diaphragms were located 190 cm forward of the main rotor teeter axis and 304 cm beneath it. The microphone booms extended 2.7 m from the centerline of the aircraft. The acoustic data from the IFAMS were recorded by two independent systems with a common 1 KHz time code.

Acoustic array instrumentation.- A schematic diagram of the noise data-acquisition system for the flyover tests is shown in figure 5. During the test program, the microphones were fitted with wind screens and positioned 1.2 m above ground surface, oriented for grazing incidence. The condenser microphones in this array had a frequency response flat to within ±3 dB over the frequency range 10 Hz to 20 000 Hz. The signal outputs from all microphones were recorded at each of the mobile data-acquisition stations on FM tape at 76.2 cm/sec using a center frequency of 54 KHz. All recorded acoustic array data contained the same time code as the onboard data systems. The frequency of the complete acoustic system was flat to ±3 dB from 10 Hz to 10 000 Hz.

TEST PROCEDURE

Evaluation of the Ogee tip shape required a systematic and controlled test environment for the measurement of acoustic signature, rotor loads, and performance. The goal of the whirl-tower tests was to explore the hover envelope of both standard and Ogee rotors. The helicopter flight tests explored those conditions which created impulsive noise through blade-vortex interactions or compressibility. In both types of testing, simultaneous measurements of rotor loads and performance were made along with acoustic data acquisition.

Whirl-tower test procedure.- The test matrix for hover on the whirl tower involved thrust values from 0 to 44 480 N (10,000 lb) at several tip Mach numbers. Table V shows the test conditions for both rotors on the whirl tower. For each rotor tested, the blades were tracked throughout the rpm range to be tested using a strobe-television system. The tracked and balanced blades were then subjected to the nominal conditions cited in table V. Performance and acoustic data were taken at each test point after the rotor environment became stable. The points were repeated several times. Wake flow visualization was achieved through the smoke rake shown in figure 2. High-speed movies were taken of the smoke flow entrained by the rotor wake. In hover performance cases, the average ambient wind was less than 2 knots and the tip Mach number was achieved within 1 percent.

Flight-test procedure.- The flight testing of both standard and Ogee rotors on the UH-1H helicopter encompassed the major portions of the flight envelope for that aircraft. Those flight conditions which generated significant impulsive noise were of prime interest, but numerous other flight conditions were also explored. Table VI shows the flight conditions for both rotors where all onboard data systems were acquiring data. Table VII indicates the flight conditions over the acoustic array at Wallops Flight Center. During the acoustic-array data acquisition, the aircraft was flown only at its lower nominal gross weight of 33 805 N (7600 lb). The flight-test conditions outlined in table VI contained at least 30 seconds of time-correlated data from all data systems. The conditions in table VII for the acoustic array flyovers involved positioning the aircraft over the array and tracking the position with radar. The majority of the level flights over the acoustic array were done at 30 and 61 m altitude. Descending flights were commenced approximately 2100 m from the threshold of the runway and continued approximately 300 m past the threshold with a flight path to put the helicopter at a nominal altitude of 122 m over the center of the microphone array. In general, at least two runs at each airspeed and rate of descent were flown during these flyover tests. Acoustic-array data were acquired during the entire approach and flyover for each run. Onboard data were taken during a 30-second period which included the time interval when the aircraft was directly over the array.

DISCUSSION OF RESULTS

The results of the full-scale rotor tests described above are presented in three segments. Acoustic data are shown in figures 6 to 12. Loads measurements are presented in figure 13, while performance information in hover and forward flight is contained in figures 14 and 15.

Acoustic Data

Hover acoustic data.- The overall sound pressure levels from the whirl-tower hover tests are shown in figure 6. Since blade-vortex interaction is not achieved in hover, these overall sound pressure levels represent rotational and broadband noise. The rotational noise from these rotors in hover has the expected trends with thrust and tip Mach number. It should be noted that the lower tip loading of the Ogee rotor results in a reduction of rotational noise

level, as does the thin profile at the Ogee rotor's tip. Figure 6 also indicates a greater sensitivity of Ogee rotational noise to thrust coefficient. This may result in a merging or crossover of OASPL for the two rotors at very high thrust coefficients although this point was not reached in the present test matrix. Figure 7 shows a segment from high-speed smoke movies of both rotors' wake. The operating conditions on the whirl tower are nominal, and, as shown, develop tip vortices which exhibit characteristics similar to those seen from small-scale studies (ref. 3). Specifically, the Ogee tip vortex has a larger core and is less well defined in the lower wake. This vortex diffusion will be shown to affect the impulsive noise.

Near-field rotor noise.- The noise perceived in a helicopter cabin and measured by external microphones is generated by several sources. Rotational noise and tail-rotor noise are certainly contributors to the overall acoustic energy; however, impulsive noise in the near field below the rotor is dominated by blade-vortex interaction. The directivity of this type of impulsive noise, as well as an explanation of its aerodynamic causes, is given in several references (refs. 6 and 7).

The test matrix for quantification of impulsive noise has already been described. From the onboard microphone data, peak levels of near-field impulsive noise below each rotor were found at conditions indicated in figure 8 for the moderate gross weight cases. The blade-vortex interaction impulsive-noise conditions for the standard rotor were moved to higher rates of descent for a given airspeed through the use of the Ogee rotor. This phenomenon may be due to the diffuse Ogee tip vortex requiring a closer proximity to the succeeding blades to generate impulsive noise. It should be noted that the maximum intensity of the Ogee impulsive noise below the rotor is significantly lower than the maximum noise of the standard rotor for the nominal 33 805 N case. At higher gross weights (38 253 N) the maximum near-field levels are similar for the two rotors although the contour for the Ogee continues to occur at higher rates of descent than the standard. The near-field acoustic data discussed in this section will be taken from these areas of maximum impulsive noise for both rotors at both ranges of gross weight.

Time histories of data from the advancing-blade microphone are shown in figure 9 for both rotors during rates of descent at moderate gross weights. The conditions chosen are those which were observed to bracket the strongest impulsive noise for both rotors. The strongest vortex-blade interaction occurs on the advancing side of the disk (ref. 7) and hence the advancing-side microphone data best illustrate the changes in such phenomena. The Ogee rotor significantly reduces this type of near-field impulsive noise as well as the rotational and tail-rotor noise in some rates of descent. (See fig. 9(a).) The rotational noise difference has been addressed in the last section. The tail-rotor noise is a function of power required and, as will be shown, significant reductions in tail-rotor power for the Ogee main rotor may be realized for some gross weights and flight conditions. Tail-rotor interactions with the main-rotor wake also cause changes in the acoustic signature of the tail rotor which are dependent on the wake's strength and trajectory.

For the higher gross-weight conditions, figures 10(a) and 10(b) bracket the strongest impulsive noise for both rotors. Figure 10(a) shows the loudest near-field impulsive level for the standard rotor while figure 10(b) indicates the Ogee trend through its loudest near-field condition. For both airspeeds shown, the Ogee peak impulsive noise occurs at a significantly higher rate of descent than the standard rotor. It should be noted that all near-field data in this study are uncorrected for atmospheric density effects. A relation which normalizes acoustic pressure to a given atmospheric density (ref. 6, eq. B-1) can be applied to the near-field data. The difference between the acoustic pressure observed at altitude and that normalized to sea level standard conditions never exceeded 2 dB for each rotor. Most data points never varied more than 0.5 dB from the normalized value. Since both rotors were flown at the same nominal range of density altitudes for this study, differences between standard and Ogee impulsive-noise levels due to variations in density are not significant.

Near-field impulsive noise for both standard and Ogee rotors contain energy souces at many harmonics. Spectrum plots of the near-field data were made using a digital analyzer operating on 2048 points from 0 to 1000 Hz. Figure 11(a) contains the spectra corresponding to the flight conditions and data of figure 9(a). The most noted changes between rotors in harmonic content occur at 250 and 1000 Hz. The absence of Ogee acoustic energy at these frequencies is due to the reduction afforded in impulsive noise by the Ogee rotor at this flight condition.

The flight condition and acoustic time histories of figure 9(b) indicated a 5.1 dB reduction in near-field impulsive noise with the Ogee tip. The corresponding spectra, figure 11(b), show that this reduction occurs mainly at 250 Hz and 1000 Hz. When the near-field impulsive noise of the two rotors are within 1 dB, such as shown in figure 9(c), the corresponding spectra (fig. 11(c)) indicate that any acoustic differences between rotors occur in the high harmonics.

Blade-to-blade acoustic variability, shown by the standard-rotor pressure time histories, has been observed in previous research efforts such as reference 6. The spectra just discussed show this variability in the frequency domain. Specifically, the standard-rotor 1-per-rev predominant-impulsive spike contrasts with the Ogee 2-per-rev trace. The width of the individual spectrum pulses shows this phenomenon.

Far-field rotor noise.- Flight tests over an acoustic array result in data as shown in figures 12(a) to 12(e). These time histories show not only the acoustic phenomena illustrated in the near-field data, but also a significant addition to the acoustic energy, impulsive noise generated by compressibility. This very directional (ref. 6) noise is shown by area A in figures 12(a) and 12(b) for level flight. The aerodynamic cause of these negative pressure pulses is discussed in references 6, 7, and 8. The compressibility noise spikes (area A) for each rotor show differences which are magnified as aircraft speed increases. Figure 12(a) shows this for level flight where compressibility on the advancing blade is maximized. The thin profile of the Ogee rotor seems to decrease the magnitude of the compressibility impulsive noise. For a low-

speed, nominally level flight condition, the difference in far-field noise between rotors is not as dramatic (fig. 12(b)) but is still significant.

During rates of descent, the blade-vortex interactions generate the signature in area B of figure 12(c) as well as the compressibility spikes (area A). The trend of the vortex-blade interaction far-field noise with rates of descent and rotor tip shape is similar to near-field trends discussed earlier. Specifically, figure 12(c) shows a case where near-field data (fig. 9(d)) indicated high standard-rotor impulsive noise whereas Ogee near-field impulsive noise at this condition was significantly less. The acoustic difference is also shown by the far-field data. Figure 12(d) presents a case where Ogee and standard near-field impulsive noise (fig. 9(c)) was shown to be nearly equal. However, this flight condition produced a measurable difference in far-field acoustic energy between the rotors with the Ogee rotor noise being less impulsive. At certain portions of the flight regime, notably, high rates of descent, the Ogee rotor can produce far-field blade-vortex impulsive noise that is comparable to the standard, although both levels are fairly low. Figure 12(e) shows the far-field noise for the two tip shapes during such a flight condition.

Rotor Loads

The character of a rotor's structural loads is very dependent on the local aerodynamic environment. The rotating pitch-link loads of both Ogee and standard rotors are shown in figures 13(a) to 13(d) for level flight. The rotors are matched in $\bar{C}_L$ within 3 percent. It may be noted in figure 13 that the trend of pitch-link load/density ratio with V_t for each rotor is similar. The significant control load differences between rotors at the low values of $\bar{C}_L$ are not as pronounced at higher $\bar{C}_L$ magnitudes (figs. 13(a) and 13(d), respectively). The reduction in peak-to-peak pitch-link loads for the Ogee rotor in level flight is probably due to a reduction in local tip chord.

Rotor Performance

Hover performance.- Hover-test data from the Langley whirl tower are shown in figures 14(a) to 14(c) for three tip Mach numbers. At low and moderate values of thrust coefficient, the performance of the Ogee rotor exceeds that of the standard. This is probably due to a substantial decrease in torque-weighted solidity for the Ogee tip while thrust-weighted solidity is only moderately decreased. At high thrust coefficient values, the performance of the two rotors merges. The value of thrust coefficient at which this occurs increases with decreasing tip Mach number. Specifically, the standard sea-level thrust values below which the Ogee is more efficient are 35 744 N (8036 lb) for 0.714 tip Mach number and 40 588 N (9125 lb) for a tip Mach number of 0.657. When both rotors were stalled in hover at low rpm ($M_{TIP} = 0.535$), the Ogee tip rotor performance line diverged from that of the standard rotor. The probable cause of this is the absence of sufficient thrust-weighted solidity needed at high thrust coefficients.

Forward flight.- Level-flight performance for standard and Ogee rotors as measured on the UH-1H test helicopter is indicated in figures 15(a) to 15(d). Thrust coefficients and tip Mach numbers were matched between rotors at a given airspeed with no greater than 3 percent difference in $\bar{C}_L$ between rotors in any figure. The trends of power coefficient with V_t for each rotor are similar at low and moderate speeds. At high speeds, the Ogee rotor C_p is more dependent on $\bar{C}_L$ than is the standard rotor.

The performance data for moderate thrust coefficients (figs. 15(a) and 15(b)), show a significant improvement in performance with the Ogee rotor throughout the speed range. This is probably due to profile power differences between the two rotors. At a $\bar{C}_L$ of 0.00361 (fig. 15(c)), the Ogee is more efficient at high speed, nearly coincident in C_p at cruise, and less efficient than the standard at low speeds. This low-speed trend continues at higher $\bar{C}_L$ (fig. 15(d)) and is probably due to the reduced thrust-weighted solidity of the Ogee rotor. The improvement in forward-flight performance, when it occurs, is due to a substantial decrease in torque-weighted solidity for the Ogee tip, while thrust-weighted solidity is only moderately decreased.

CONCLUDING REMARKS

Full-scale tests were utilized to investigate the effects of the Ogee tip on helicopter rotor acoustics, loads, and performance. A whirl tower and an instrumented UH-1H were used for this study. From the data analyzed to date, the Ogee tip changed the characteristics of the standard UH-1H rotor as follows:

1. The impulsive noise caused by vortex-blade interaction and compressibility was reduced for many flight conditions tested. Blade-vortex interaction noise was reduced by as much as 15 dB.

2. Rotational noise in hover was reduced throughout the thrust range tested on the whirl tower.

3. Oscillatory control loads were reduced by as much as 50 percent.

4. Forward-flight performance was significantly increased through use of the Ogee tip for some flight conditions.

5. Whirl-tower hover performance of the standard rotor was improved by the Ogee tip for low and moderate thrust coefficients. The performance advantage was dependent on tip Mach number and was eliminated at high values of thrust coefficient.

6. The tail-rotor noise was lower for many flight conditions with the Ogee tip main rotor.

REFERENCES

1. Ward, John F.; and Young, Warren H., Jr.: A Summary of Current Research in Rotor Unsteady Aerodynamics with Emphasis on Work at Langley Research Center. AGARD Conference Proceedings No. 111 on Aerodynamics of Rotary Wings, Fluid Dynamics Panel Specialists' Meeting (Marseilles, France), Sept. 13-15, 1972. pp. 10.1-10.20.

2. Balcerak, John C.; and Feller, Raymond F.: Vortex Modification by Mass Injection and by Tip Geometry Variation. USAAMRDL Tech. Rept. 73.45, 1973.

3. Landgrebe, Anton J.; and Bellinger, E. Dean: Experimental Investigation of Model Variable-Geometry and Ogee Tip Rotors. NASA CR-2275, 1974.

4. Balcerak, John C.; and Feller, Raymond F.: Effect of Sweep Angle on the Pressure Distributions and Effectiveness of the Ogee Tip in Diffusing a Line Vortex. NASA CR-132355, 1973.

5. Rorke, James B.; and Moffitt, Robert E.: Wind Tunnel Simulation of Full Scale Vortices. NASA CR-2180, 1973.

6. Schmitz, F. H.; and Boxwell, D. A.: In-Flight Far-Field Measurement of Helicopter Impulsive Noise. J. of Am. Helic. Soc., vol. 21, no. 4, Oct. 1976, pp. 2-16.

7. Tangler, James L.: Schlieren and Noise Studies of Rotor in Forward Flight. Preprint 77.33-05, 33rd Ann. Nat. Forum of the Am. Helic. Soc., (Washington, DC), May 1977.

8. Farassat, F.: Theory of Noise Generation from Moving Bodies with an Application to Helicopter Rotors. NASA TR R-451, 1975.

TABLE I.- WHIRL-TOWER CHARACTERISTICS

Rotor height from ground	12.8 m (42 ft)
Available power	1.119 MW (1500 hp)
Type of rotor drive	Electric motor

TABLE II.- TEST ROTOR CHARACTERISTICS

	STANDARD	OGEE
Type of hub	Teetering	Teetering
Rotor radius	7.315 m (24 ft)	7.315 m (24 ft)
Blade chord	53.34 cm (21 in.) Constant	53.34 cm (21 in.) Varying
Blade airfoil	0012	0012
Blade twist (root to tip)	-10.9^{o} Linear	-10^{o}
Precone angle	2.375^{o}	2.375^{o}
Number of blades	2	2
Rotor nominal rotational speed	324 rpm	324 rpm
Rotor solidity	0.04655	0.04412

TABLE III.- WHIRL-TOWER INSTRUMENTATION AND ACCURACIES

INSTRUMENTATION

Parameter	Sensor
Thrust	Load cells
Torque	Strain-gage bridge
Angular velocity	Photo counter
Thrust correction	Strain-gage bridge
Collective pitch angle	Potentiometer
Ambient temperature	Thermocouple
Static pressure	Barometer
Blade loads	Strain-gage bridges

ACCURACIES

Rotational speed, rpm	± Thrust coefficient accuracy	± Torque coefficient accuracy
324	3.5×10^{-5}	1.12×10^{-6}
291	4.35×10^{-5}	1.39×10^{-6}
240	6.39×10^{-5}	2.05×10^{-6}

TABLE IV.- FLIGHT DATA PARAMETERS

PARAMETER	SENSOR	DATA TYPE	ACCURACY*
• Three vehicle attitudes	Gyro	PCM	1.0%
• Three angular rates	Gyro	PCM	1.0%
• Three linear accelerations	Accelerometer	PCM	1.0%
• Four control inputs	Transducer	PCM	1.0%
• Angle of attack	Vane/potentiometer	PCM	1.0%
• Angle of sideslip	Vane/potentiometer	PCM	1.0%
• Main rotor blade angle	Control position transducer	PCM	1.0%
• Main rotor azimuth	Shaft encoder	PCM	1.0%
• Total temperature	Hot wire	PCM	1.0%
• Static/differential pressure	Pressure transducer	PCM	1.0%
• Main rotor speed	Magnetic counter	PCM	1.0%
• Engine torque pressure	Pressure transducer	PCM	1.0%
• Rate of climb	Inertial vertical speed indicator	PCM	1.0%
• Chordwise bending moment at stations 84 and 192 on main rotor blade	Strain gage	FM	2.5%
• Flapwise bending moment at stations 84 and 192 on main rotor blade	Strain gage	FM	2.5%
• Rotating pitch link load	Strain gage	FM	2.5%
• Time code	36-bit time code generator		
• Ogee tip joint bending moments	Strain gage	High-speed PCM	1.0%
• Ogee tip pressures	Flush-mounted pressure transducers	High-speed PCM	1.0%

*Full scale

TABLE V.- WHIRL-TOWER HOVER TEST MATRIX

Thrust, N	(lb)	RPM			
		240	291	324*	356**
0	0	↓	↓	↓	↓
8 896	(2 000)				
17 792	(4 000)				
26 688	(6 000)				
35 684	(8 000)				
44 480	(10 000)				

*Nominal aircraft operating rpm.
**Ogee rotor only.

TABLE VI.- FLIGHT-TEST ENVELOPE FOR NEAR-FIELD ACOUSTIC AND SYSTEMS DATA

INDICATED AIRSPEED, KNOTS	RATE OF DESCENT, FT/MIN*	FLIGHT CONDITION
30, 40	-25 to -200	Climb
20-120	0	Level flight
55-115	100 to 1500	Descent
50, 60, 80, 90	0 (1.5 g, 2.0 g turns)	Maneuver
0	0 (In ground effect; out of ground effect)	Hover

*1 ft/min = 0.0051 m/sec.

TABLE VII.- FLIGHT CONDITIONS OVER ACOUSTIC ARRAY

INDICATED AIRSPEED, KNOTS	RATE OF DESCENT, FT/MIN*
55, 80, 115	0
55, 70, 80, 90	100, 250, 350, 600, 1000

*1 ft/min = 0.0051 m/sec.

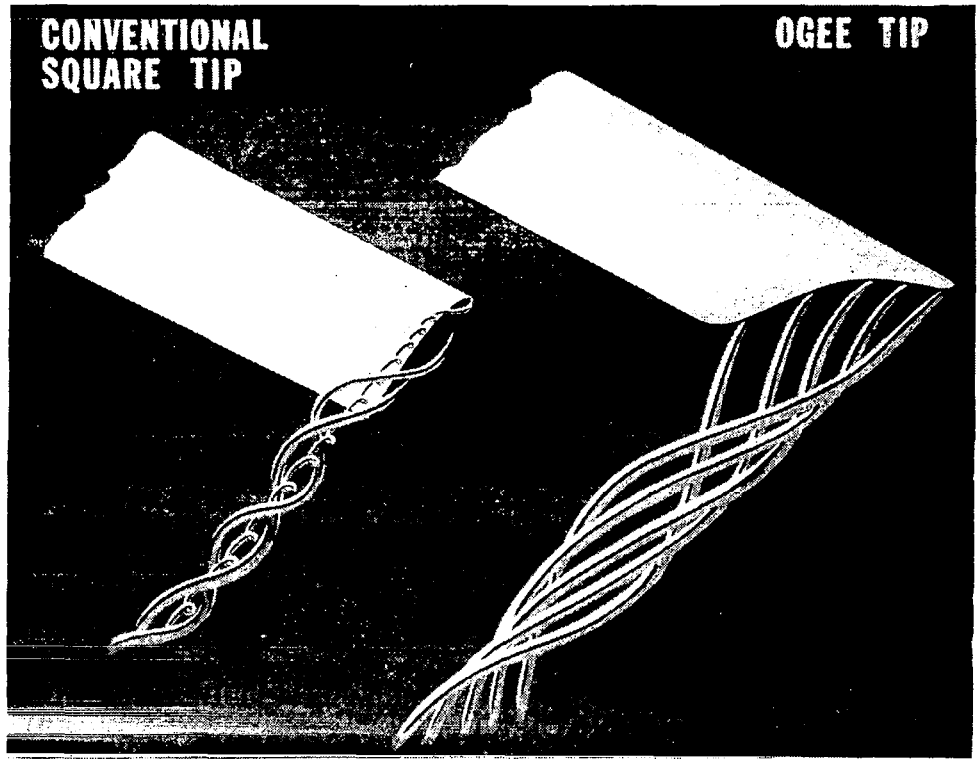

Figure 1.- Ogee planform and vortex diffusion concept.

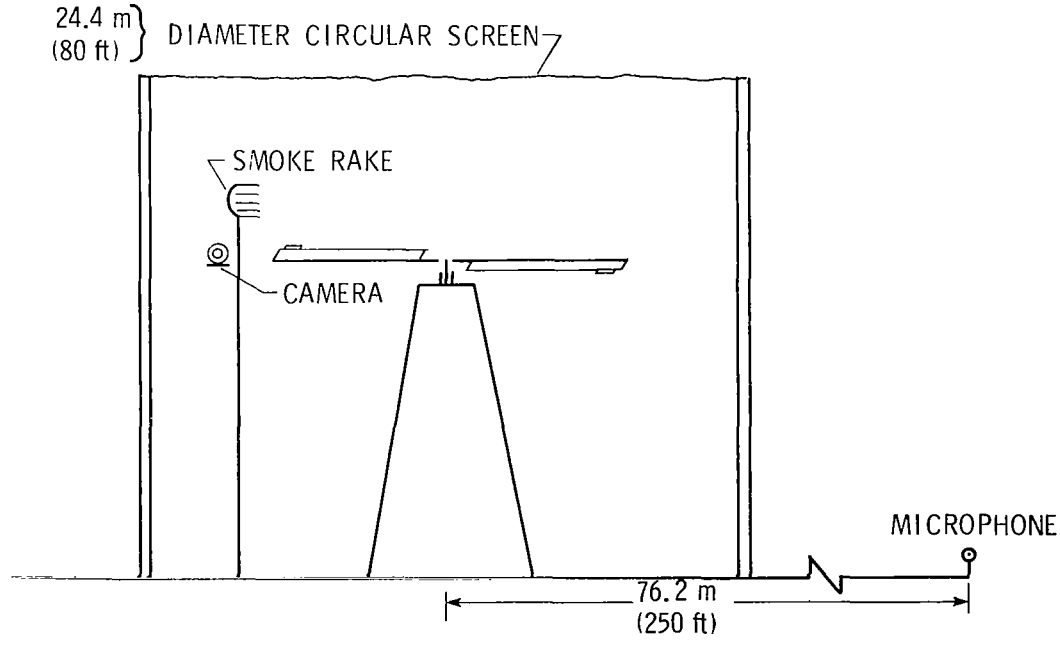

Figure 2.- Schematic of whirl-tower test apparatus.

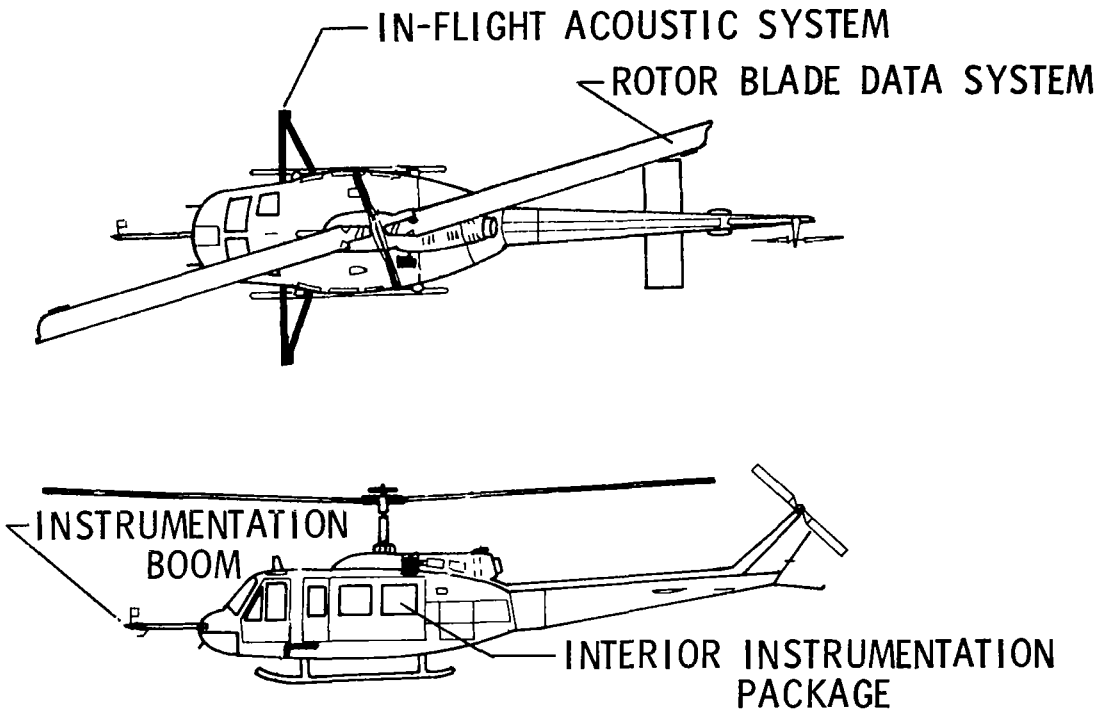

Figure 3.- UH-1H test helicopter.

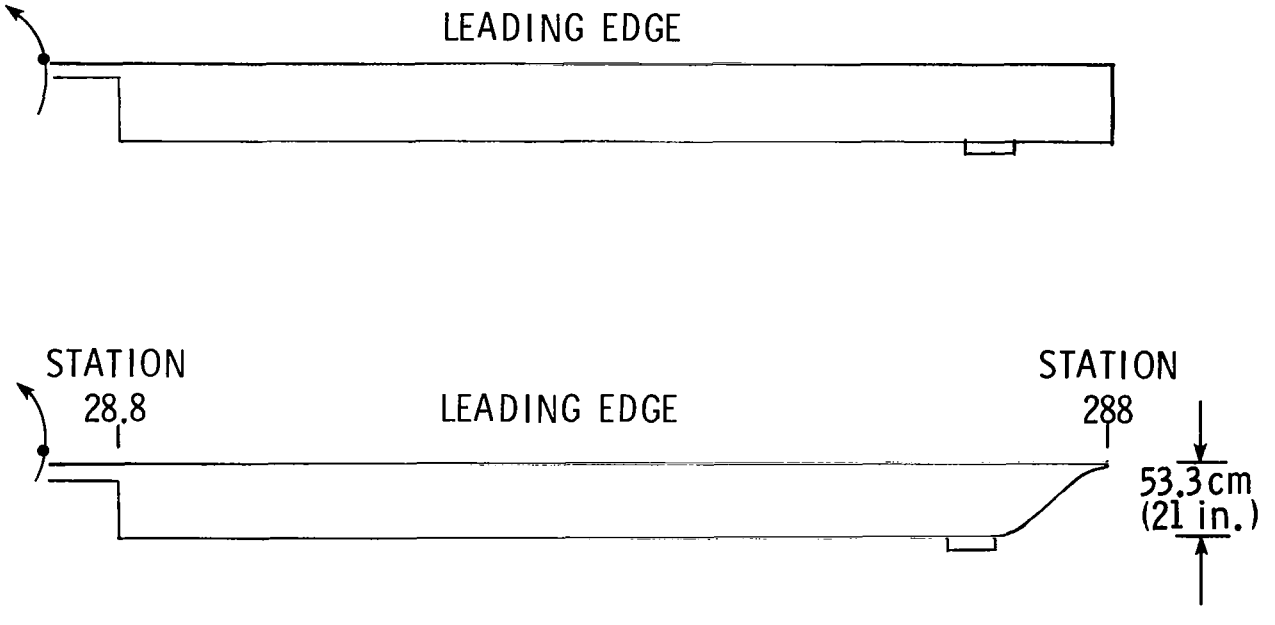

Figure 4.- Test rotor planforms.

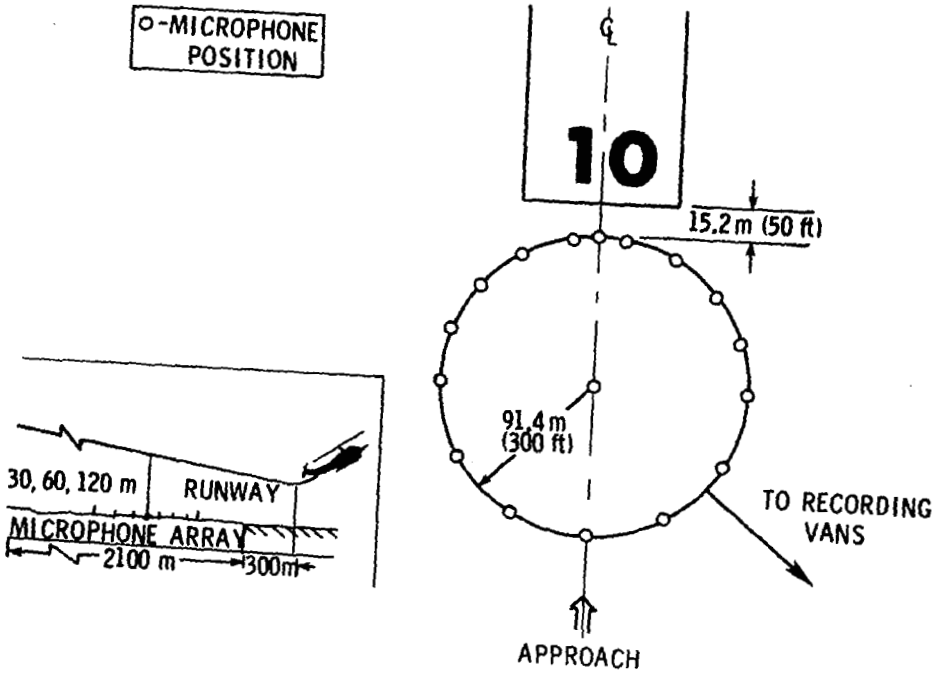

Figure 5.- Acoustic array schematic.

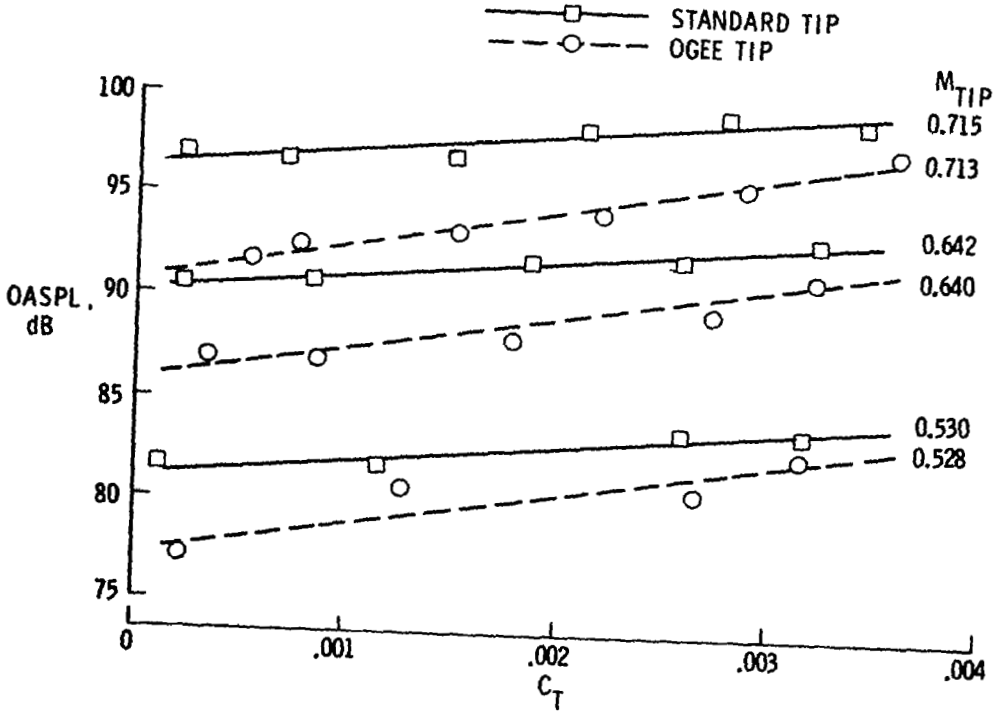

Figure 6.- Overall sound pressure levels for Ogee and standard rotors in hover.

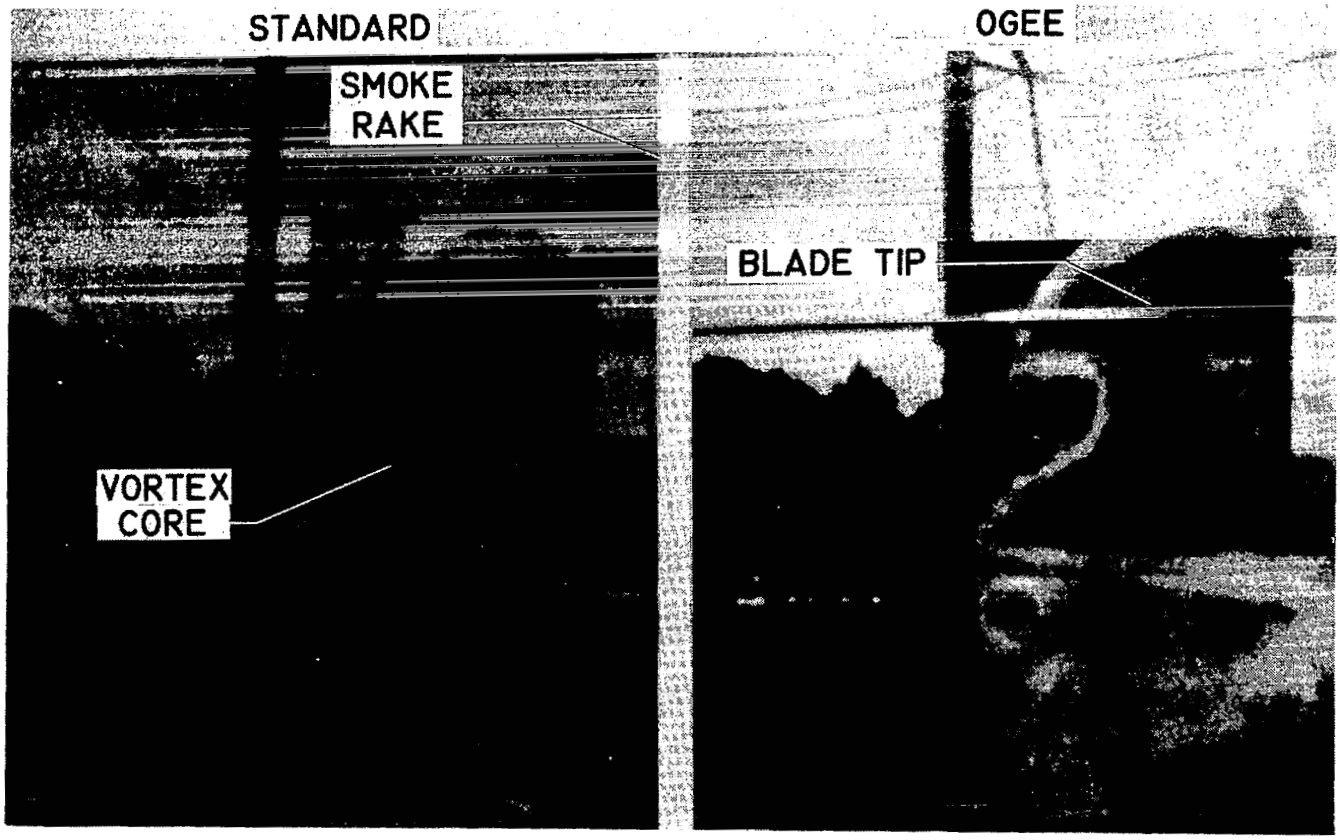

Figure 7.- Smoke flow visualization of vortex wake in hover for 35 584 N (8 000 lb) thrust at 324 rpm.

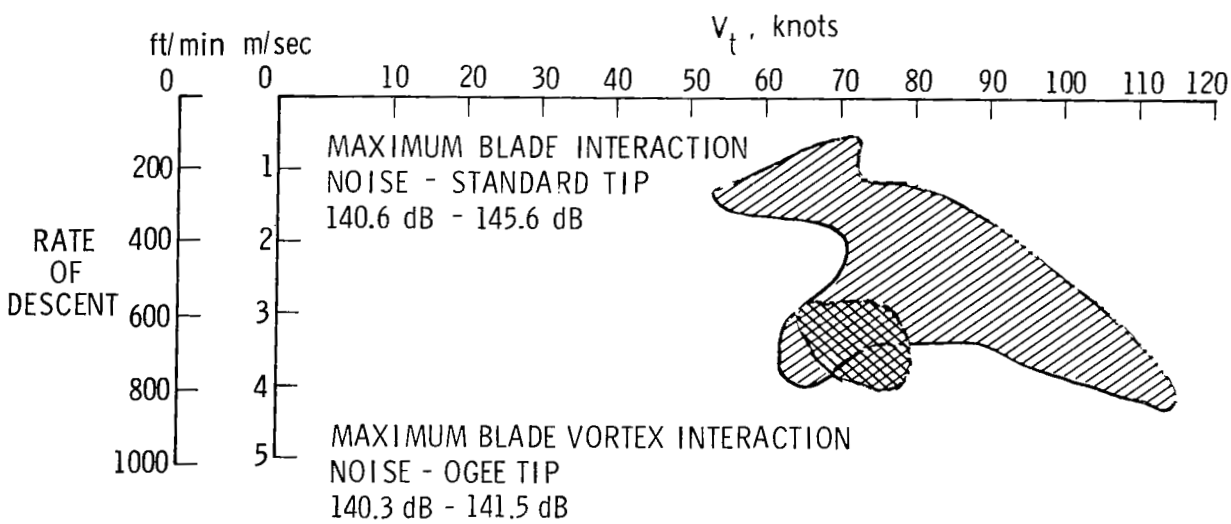

Figure 8.- Peak levels of near-field impulsive noise for nominal 33 805 N (7 600 lb) UH-1H as measured by IFAMS.

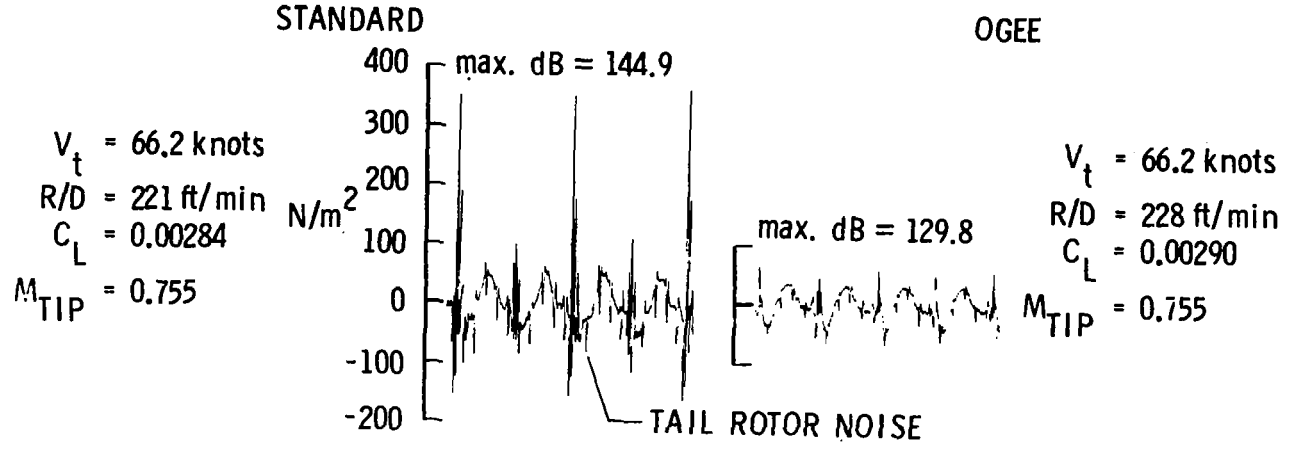

(a)

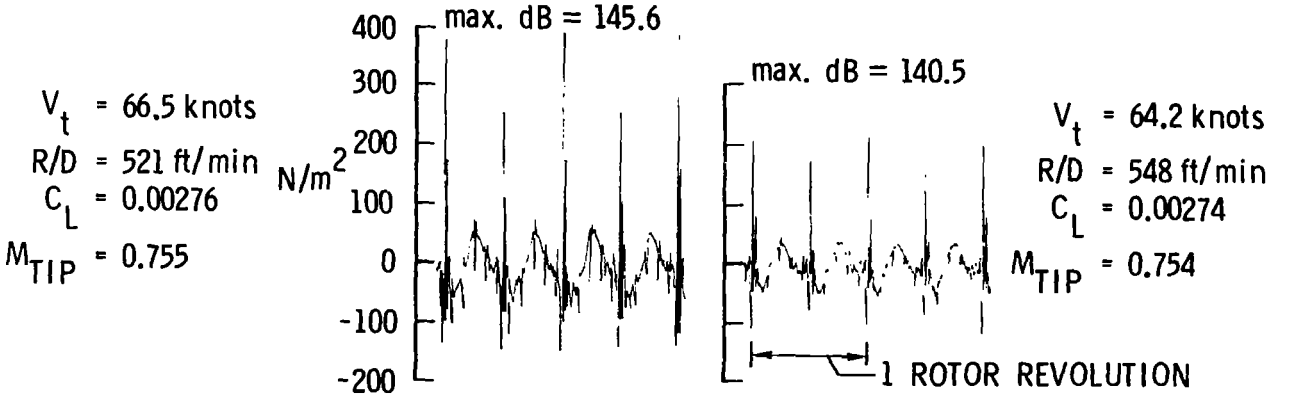

(b)

Figure 9.- Advancing-side microphone pressure time histories.

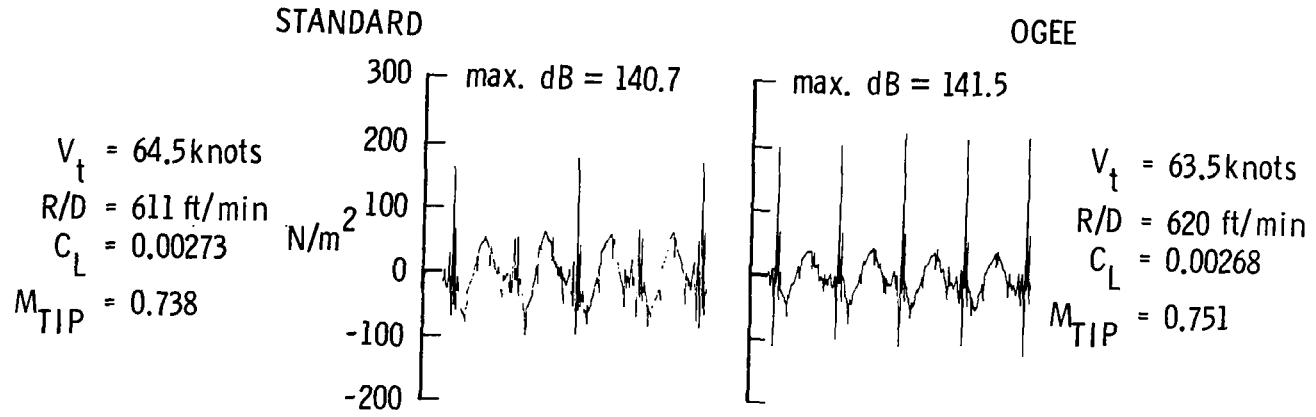

(c)

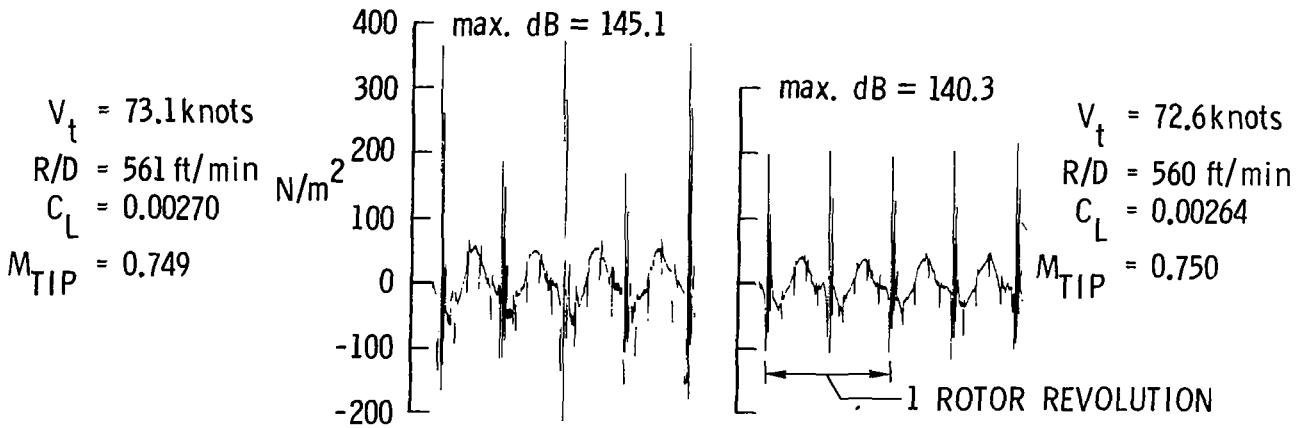

(d)

Figure 9.- Concluded.

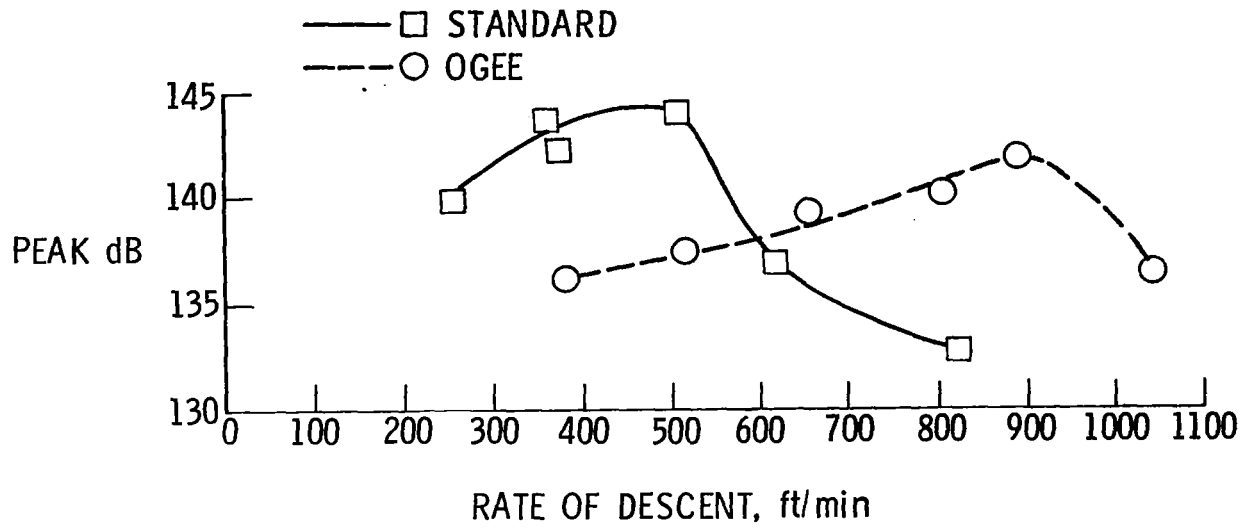

(a) $\bar{V}_t$ = 72.7 knots; $\bar{C}_L$ = 0.00309.

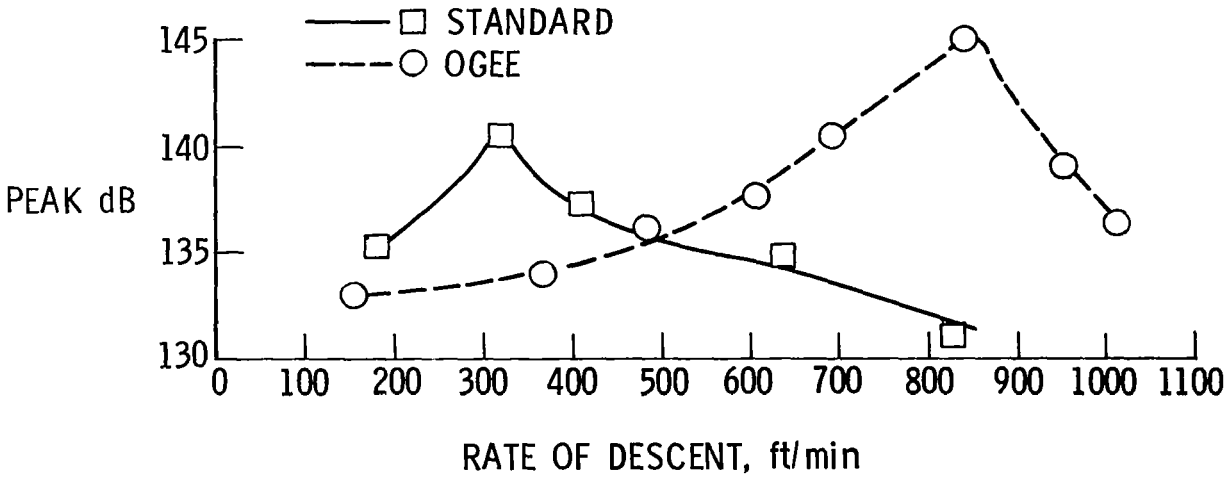

(b) $\bar{V}_t$ = 66.5 knots; $\bar{C}_L$ = 0.00306.

Figure 10.- Near-field peak sound pressure level variation with rate of descent at high gross weight.

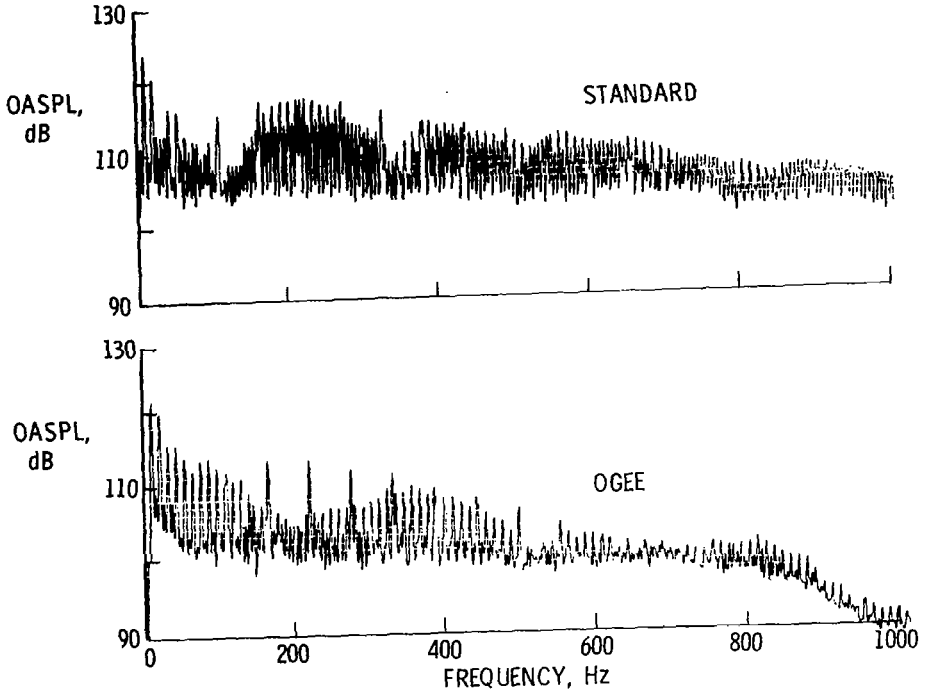

(a) Flight condition of figure 9(a).

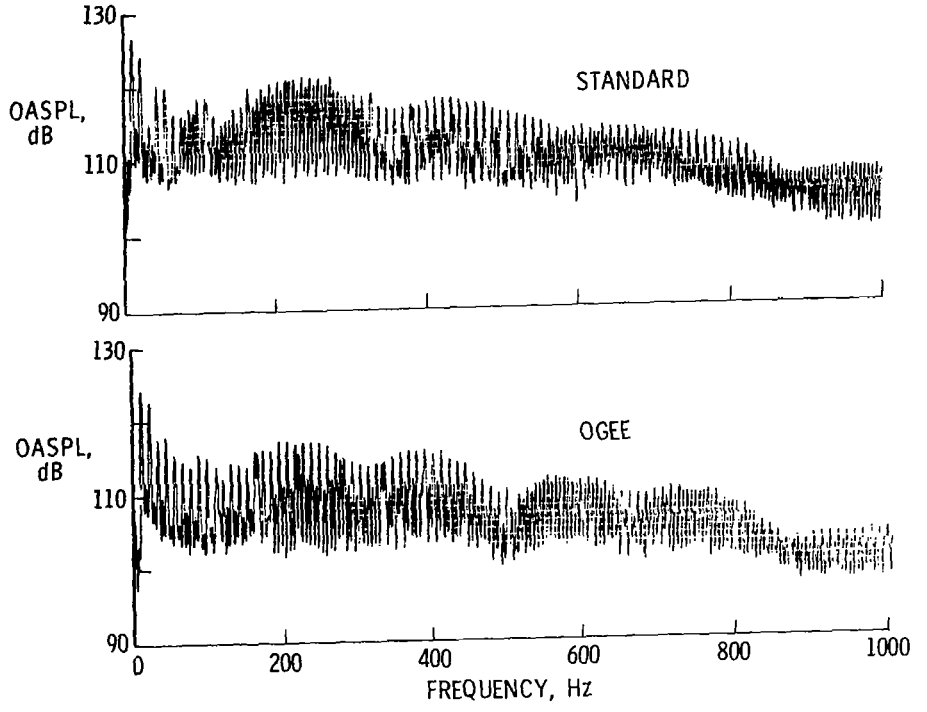

(b) Flight condition of figure 9(b).

Figure 11.- Spectra for near-field noise data.

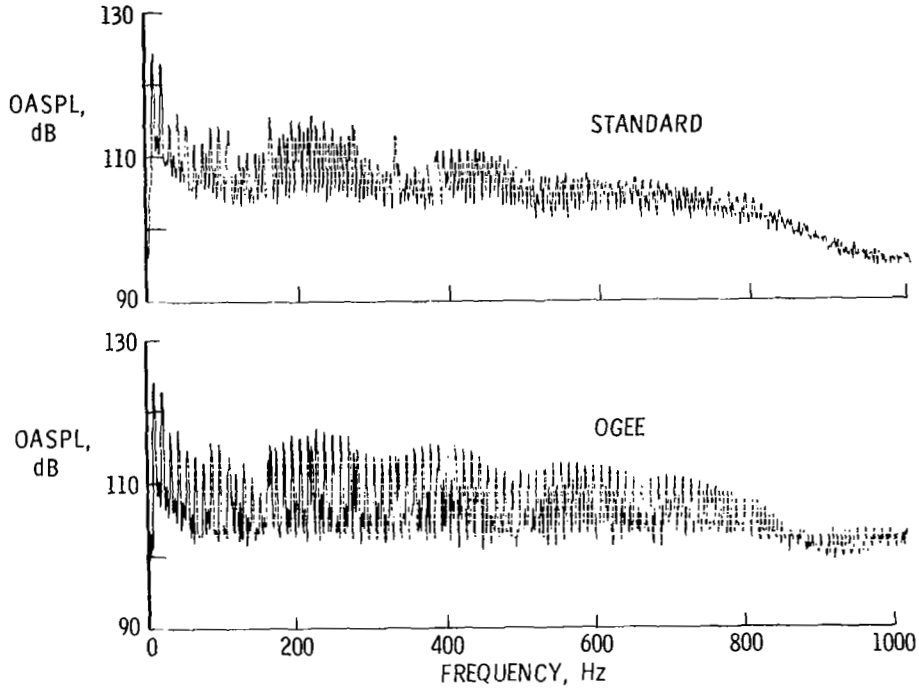

(c) Flight condition of figure 9(c).

Figure 11.- Concluded.

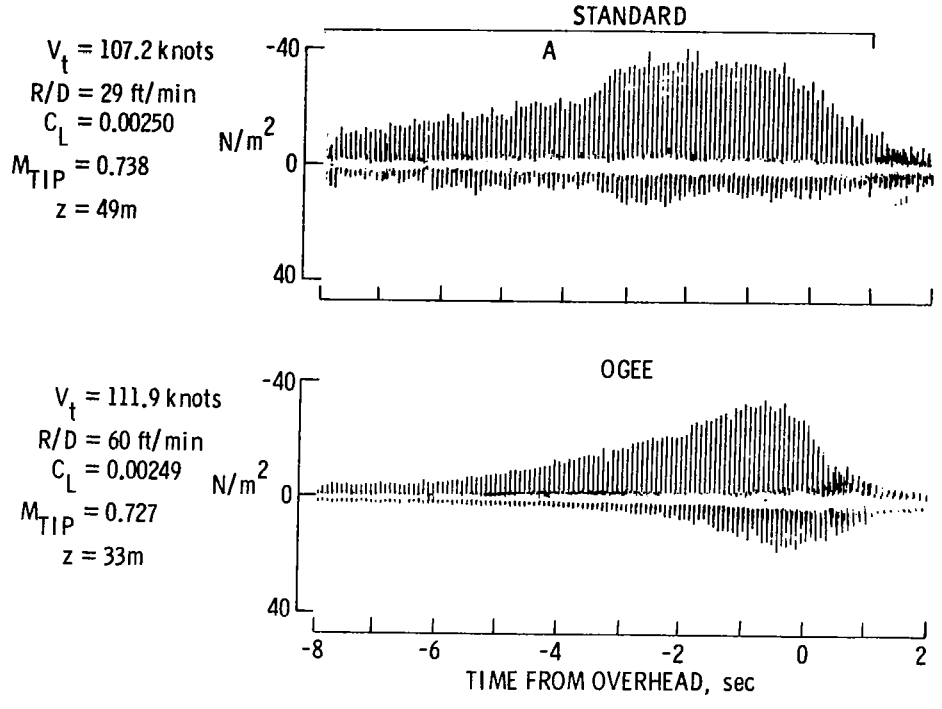

(a) High-speed level flight.

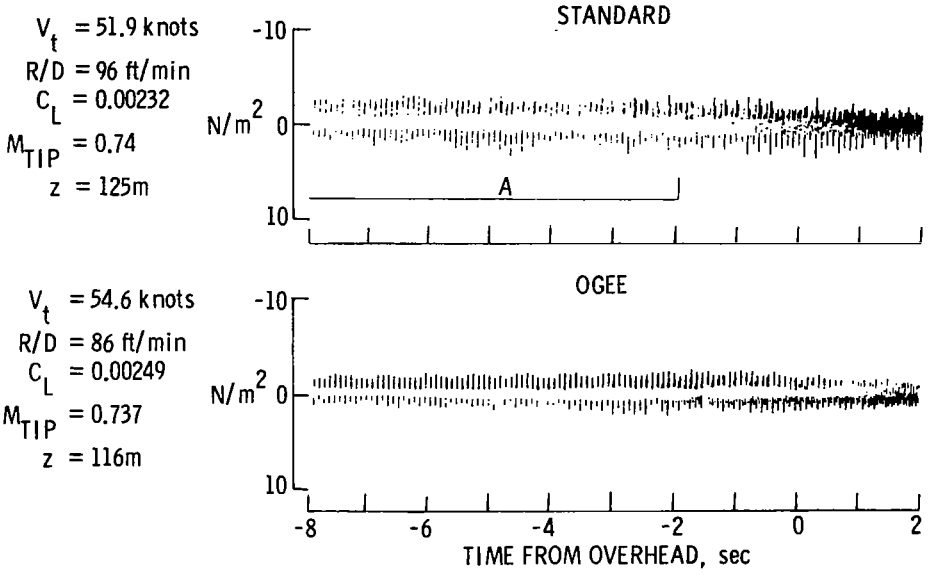

(b) Low-speed level flight.

Figure 12.- Far-field rotor noise measured by acoustic array center microphone.

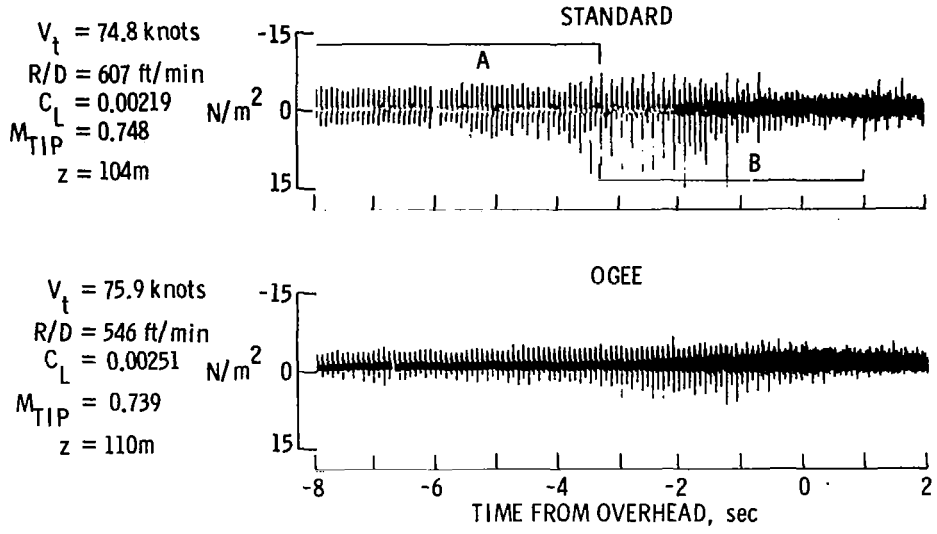

(c) Rate of descent.

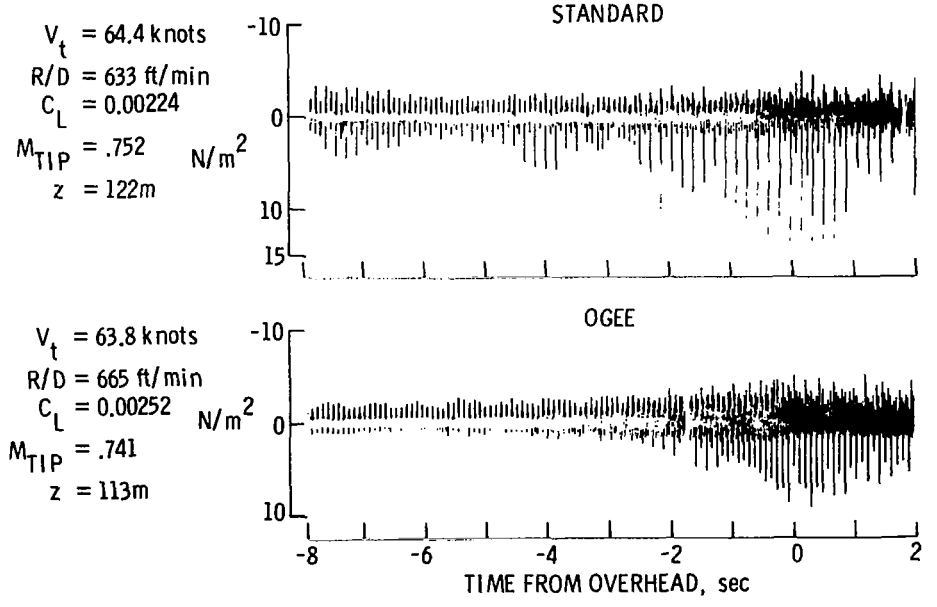

(d) Rate of descent.

Figure 12.- Continued.

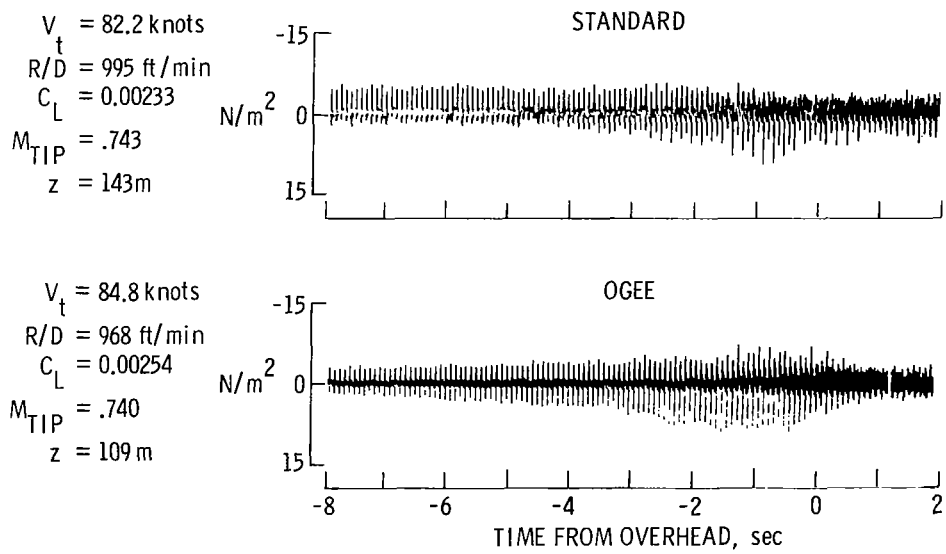

(e) High-speed high rate of descent.

Figure 12.- Concluded.

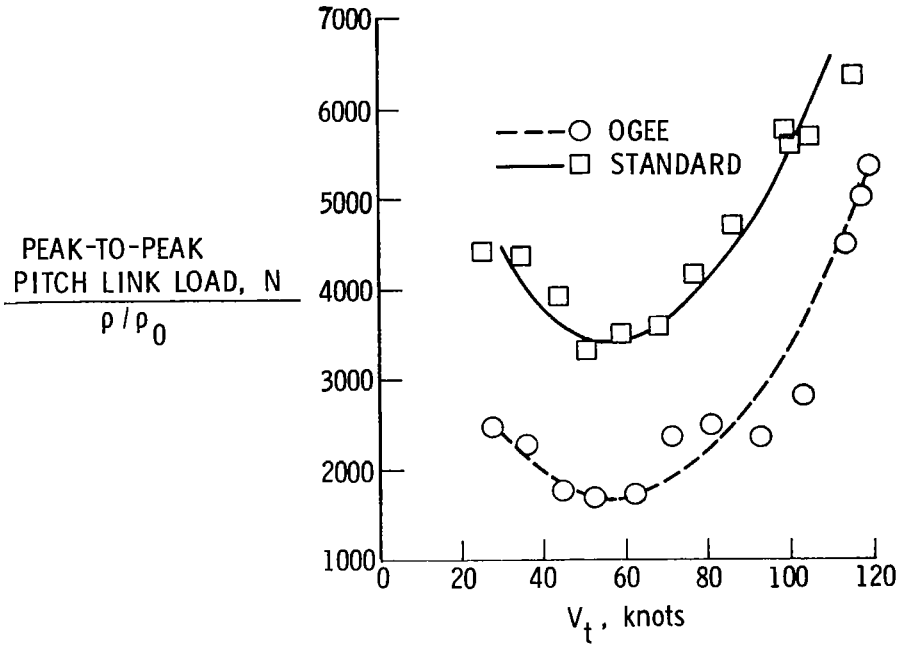

(a) $\bar{C}_L = 0.00266$; $\bar{M}_{TIP} = 0.744$.

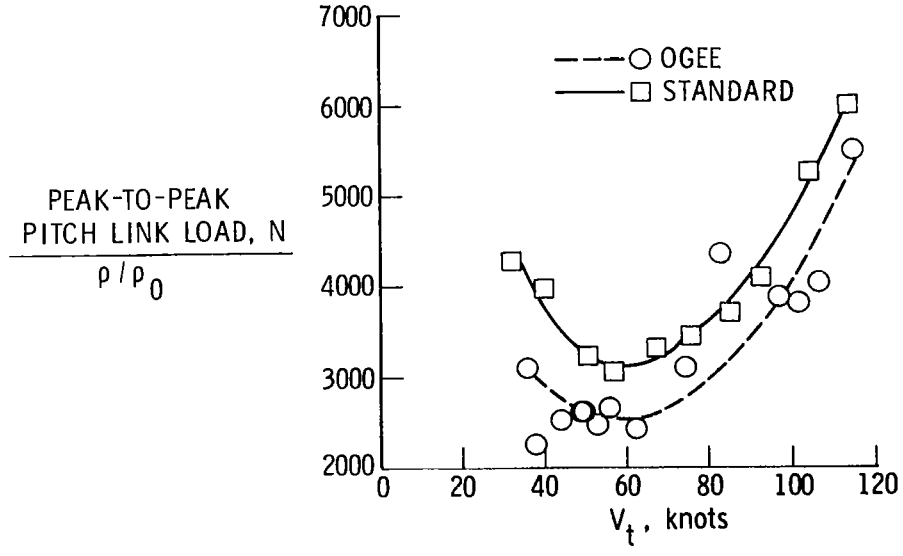

(b) $\bar{C}_L = 0.00323$; $\bar{M}_{TIP} = 0.733$.

Figure 13.- Oscillatory pitch link loads in level flight.

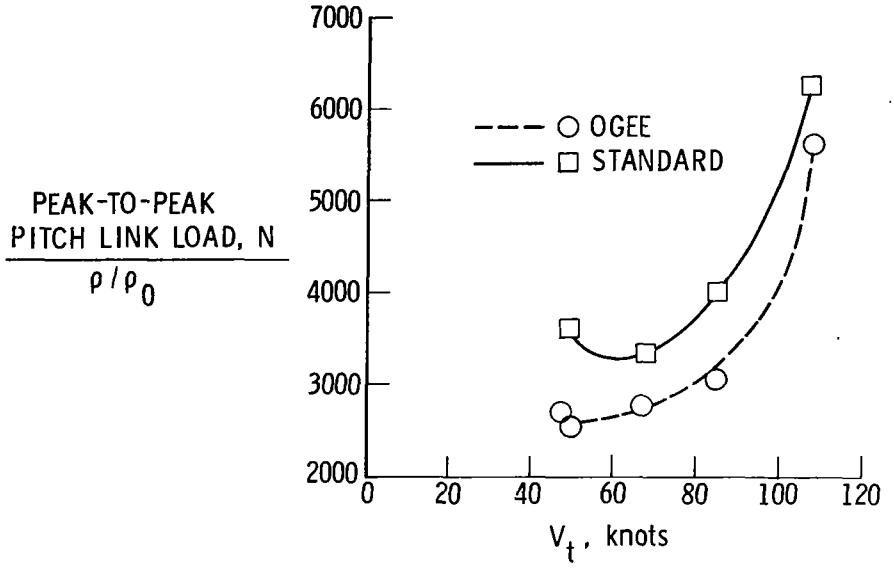

(c) $\bar{C}_L = 0.00356$; $\bar{M}_{TIP} = 0.736$.

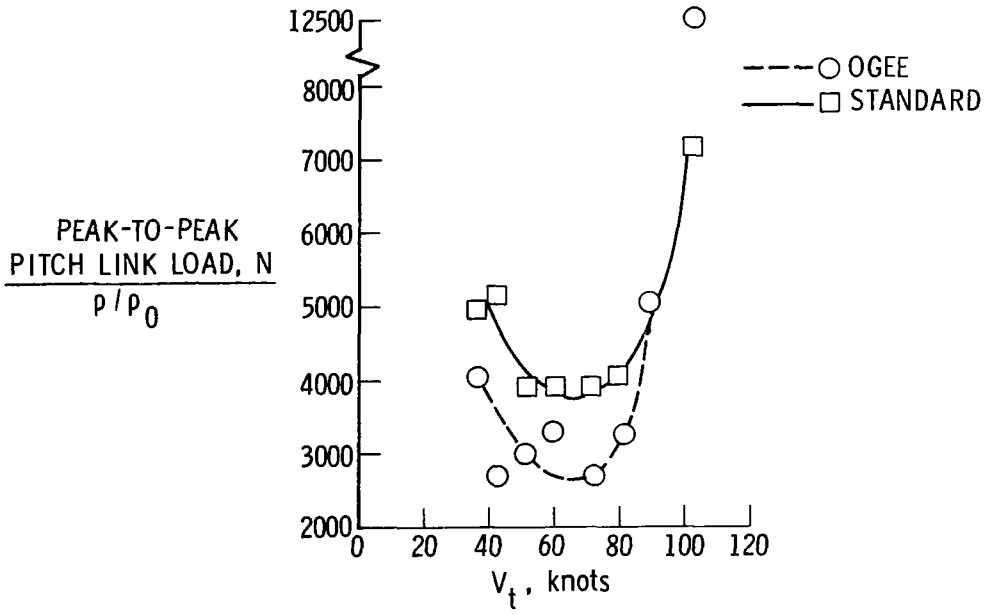

(d) $\bar{C}_L = 0.00388$; $\bar{M}_{TIP} = 0.75$.

Figure 13.- Concluded.

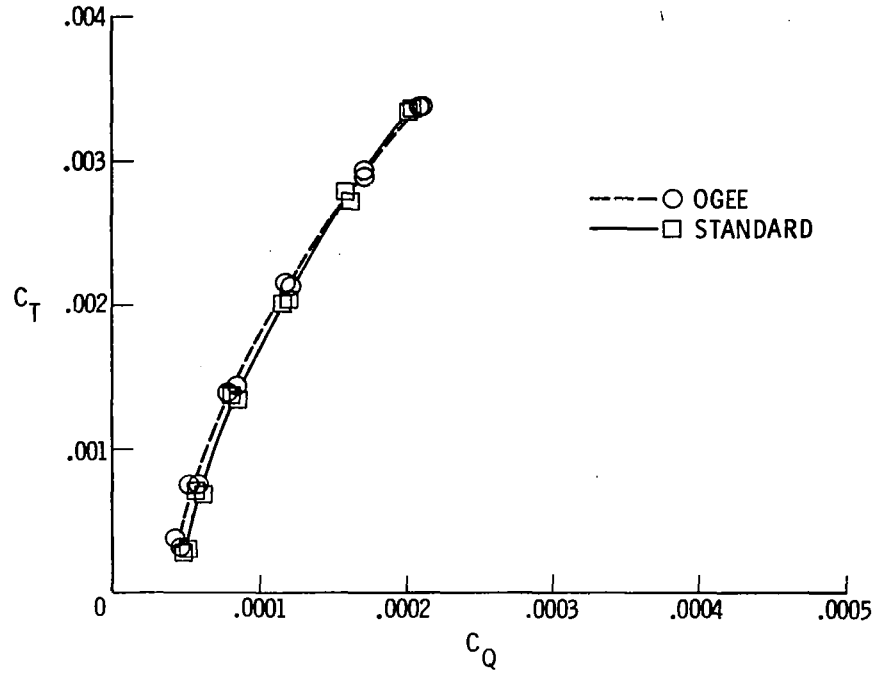

(a) $\bar{M}_{TIP} = 0.714.$

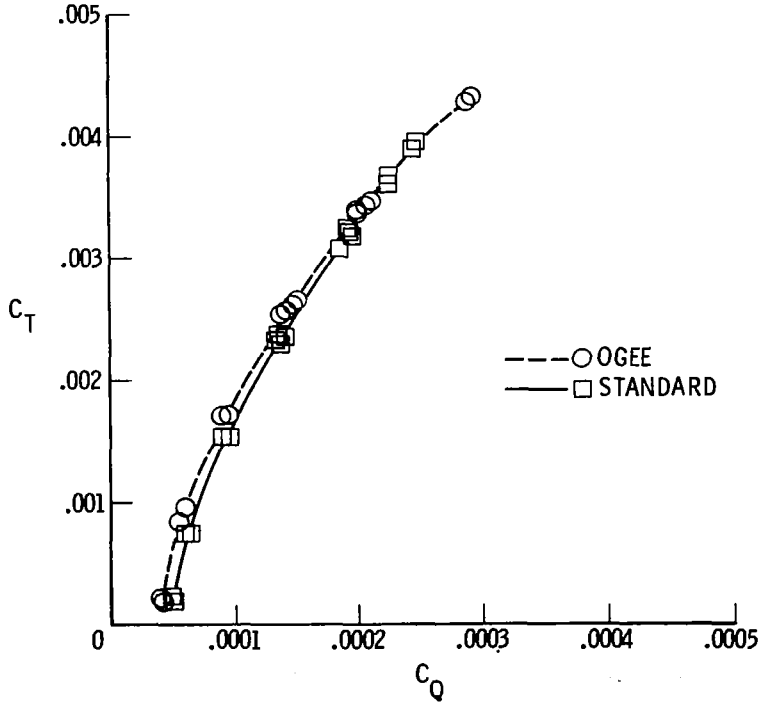

(b) $\bar{M}_{TIP} = 0.657.$

Figure 14.- Hover performance data from whirl tower.

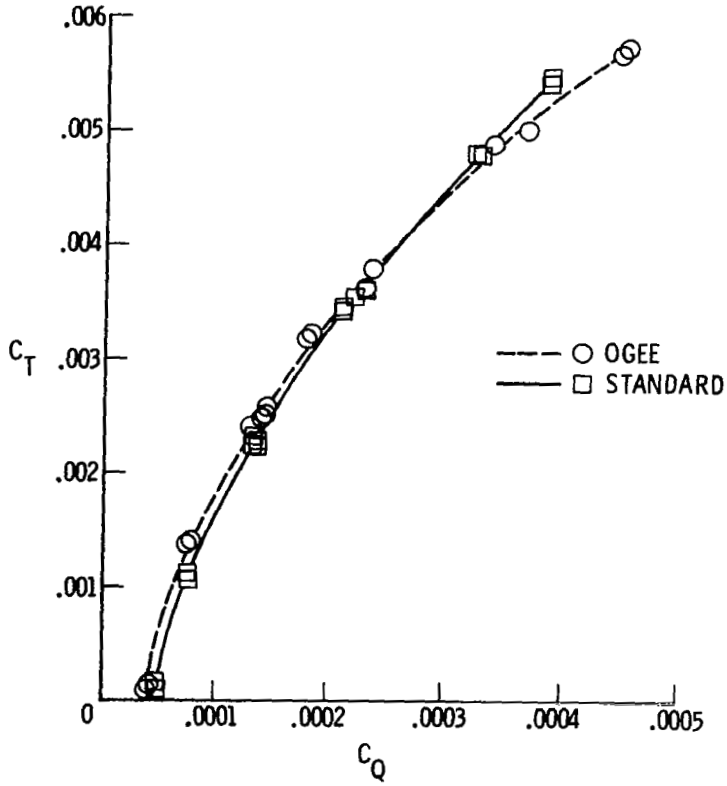

(c) $\bar{M}_{TIP} = 0.535$.

Figure 14.- Concluded.

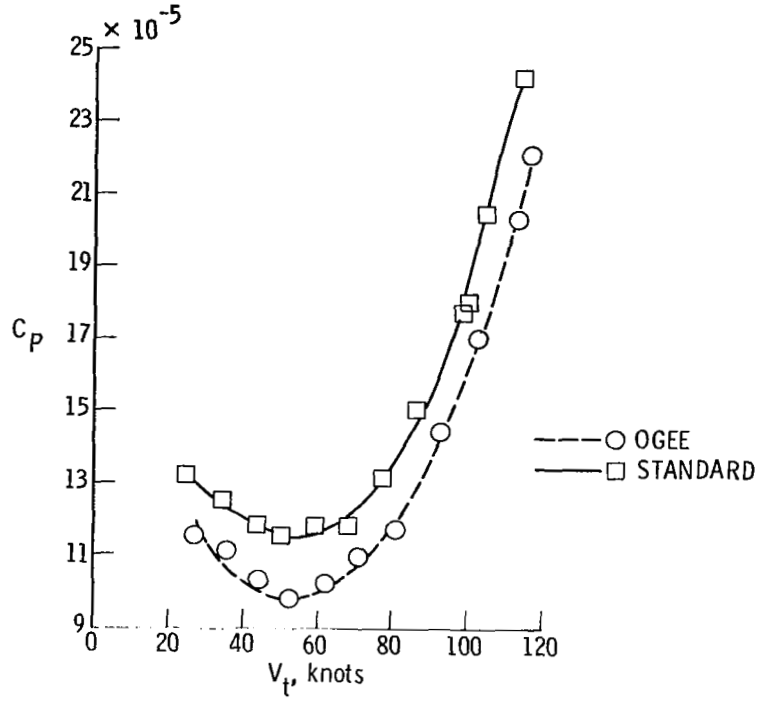

(a) $\bar{C}_L = 0.00266$; $\bar{M}_{TIP} = 0.744$.

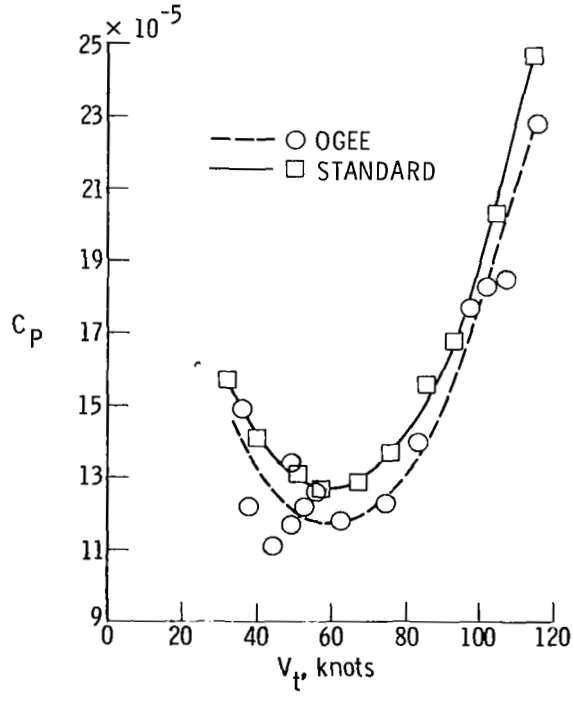

(b) $\bar{C}_L = 0.00323$; $\bar{M}_{TIP} = 0.733$.

Figure 15.- Forward-flight performance of standard and Ogee rotors.

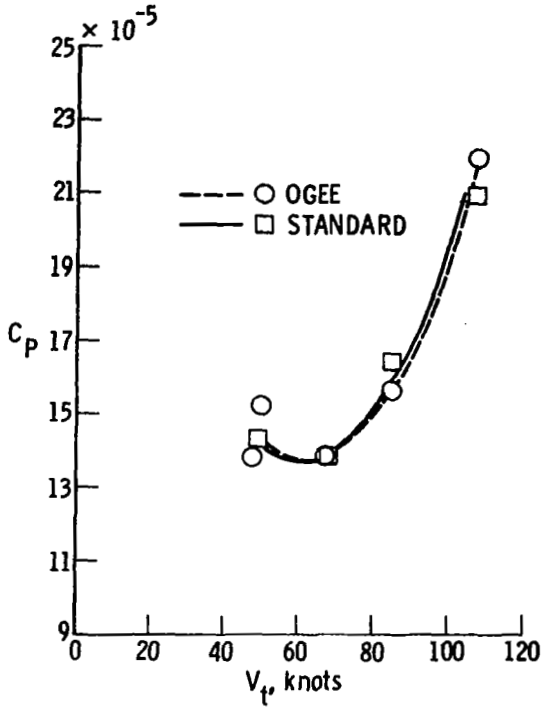

(c) $\bar{C}_L = 0.00356$; $\bar{M}_{TIP} = 0.736$.

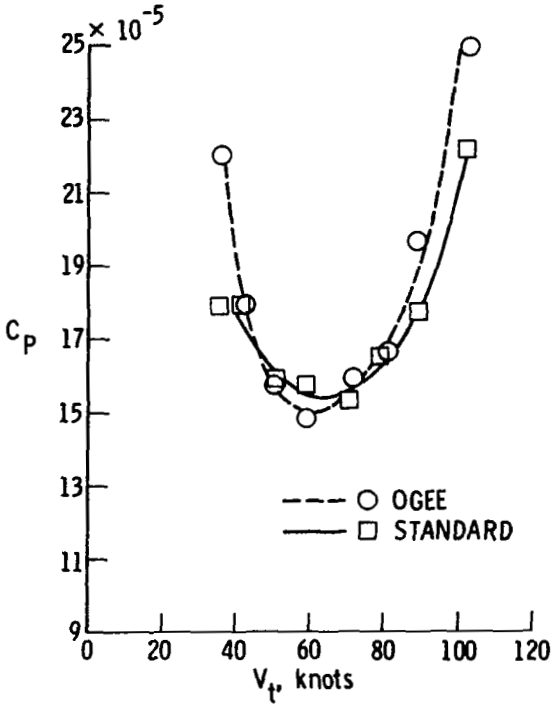

(d) $\bar{C}_L = 0.00388$; $\bar{M}_{TIP} = 0.75$.

Figure 15.- Concluded.